Effect of Mass and Geometry on the Performance of Different PM Steels after Sinter-Hardening

Yi Ding[1, a*], Ulf Engström[1, b], and Zhaoqiang Tan [1, c]

[1] Höganäs China Co. Ltd, 5646 Waiqingsong Road, Shanghai, China
[a]laurrent.ding@hoganas.com, [b]ulf.engstrom@hoganas.com,
[c]simon.tan@hoganas.com

Keywords: Sinter-Hardening, Performance, Mass, Geometry

Abstract

Sinter hardening has developed into a highly cost-effective method for the production of through hardened powder metallurgy (PM) components without the need for additional heat treatments. Over the last years, advances have been made in sinter-hardening materials, processing and with furnaces. Gas quenching can be realized when the cooling zone, directly added to the sintering furnace is prepared with the controlled cooling gas. The performance of the PM component is not only affected by the material and the process, but also by its mass and geometry. In this paper, the effect of mass and geometry on the performance of different PM components in different materials will be studied. .

Introduction

In recent years, growing demands for increased mechanical properties of powder metallurgy (PM) steels that are also cost-effective has led to significant innovations in PM [1]. Sinter hardening is a cost-effective manufacturing route for sintered parts with high performance [2-4]. Interest in sinter hardening is growing because it combines the two processes of sintering and hardening in one operation [5, 6].

A cooling zone directly added to the sintering furnace can realize gas quenching for the sintering parts from the sintering temperature with the controlled cooling rate [7]. By using a controlled post-cooling rate, the microstructures can be manipulated to form the required amount of martensite and other phases to realize the desired mechanical properties [8]. This can spare the components from oil contamination which is inevitable in oil quenching processes after sintering.

The amount of martensite in the sinter-hardening component not only depends on the hardenability of the materials, but also the cooling behavior [9]. The cooling behavior in the post-sinter cooling includes cooling gas flow, loading condition, component mass and geometry. To meet the requirements of end-users, the microstructure and performance of the sinter-hardening component should be performed precisely. In this paper, the effect of the mass and geometry of the component on the performance of

several typical sinter-hardening materials has been investigated in the controlled cooling gas flow.

Experimental

Three pre-alloyed base powders have been used in this experiment and these are shown below in Table 1.

Table 1. Chemical contents of the investigated base powders.

Grade	Cu%	Mo%	Cr%
Distaloy DH	2*	1.5	
Astaloy CrM		0.5	3
Astaloy CrA			1.8

* Diffusion bonded

The chemical contents of the mixed powders are shown in Table 2. The codes for the mixed powders used in this paper are also shown in the table. Natural graphite UF4, electrolytic copper with a 200 mesh particle size, and carbonyl nickel powder were admixed with base powder. Lube E was used as lubricant.

Table 2 Chemical contents of the mixed powders.

Base powder	Code	C%	Cu%	Mo%	Cr%	Ni%	Lub.%
Distaloy DH	DH	0.6	2	1.5			0.6
Astaloy CrM	CrM	0.45		0.5	3		0.6
Astaloy CrA	CrANi	0.8			1.8	2	0.6
Astaloy CrA	CrACu	0.8	1		1.8		0.6

* Diffusion bonded ** Admixed

The gear specimens were compacted by an 800 ton, hydraulic CNC press with two upper punches and two lower punches, to the nominal density of 7.0 g/cm^3 through a conventional compaction method. It is important to note that the compaction pressure has been varied considerably for the selected base materials and the geometry of the gear specimens in order to achieve the desired density. The sketches of the gear specimens are shown in Figure 1. The three gear specimens with different dimensions and geometries are identified as Gear A, Gear B and Gear C, respectively.

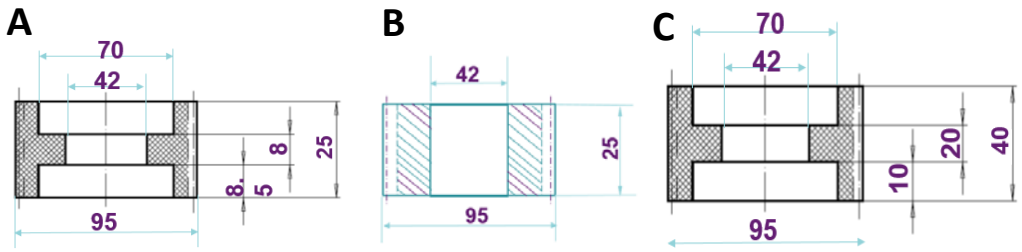

Fig. 1. Sketch of the gear specimens.

The compacted green Gear A is shown in Figure 2. The mass of the gear specimens was measured using the Hengjia Electronic Scale.

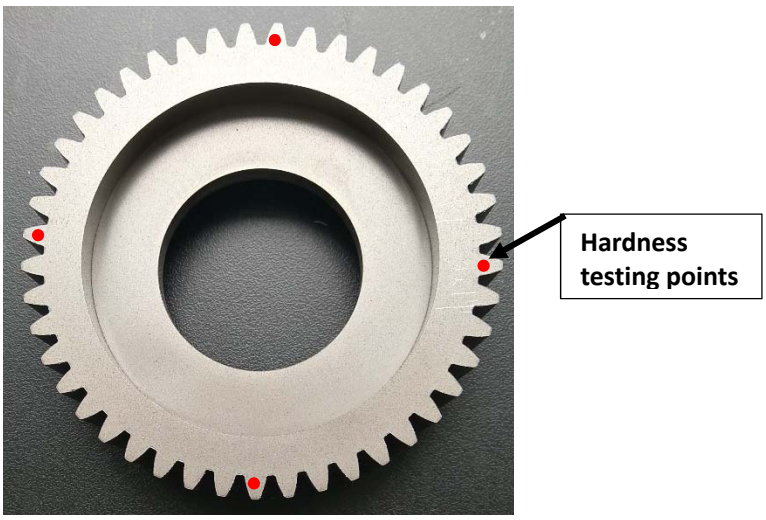

Fig. 2. Green specimen of Gear A and distribution of the apparent hardness testing points.

Sintering was performed in a newly designed push-plate furnace equipped with a rapid cooling system following the sintering area to realize the soft quenching with the cooling rate up to 8 ℃/s using a controlled cooling gas. The sintering temperatures used in this study were set to 1120 ℃ and 1250 ℃. Sintering time was 30 mins at the sintering temperature and the atmosphere was 90/10 nitrogen and hydrogen.

A cooling fan controlled the cooling rate with a controllable rotation speed up to 50Hz. An illustration of the cooling system is shown in Figure 3. The relationship between the rotation speed of the fan and the cooling rate, determined by metallographic investigation of the TS bars, is shown in Figure 4. Fan rotation speeds of 5 Hz, 15 Hz and 35Hz were used with corresponding cooling rates of 0.8 ℃/s, 3 ℃/s and 6 ℃/s.

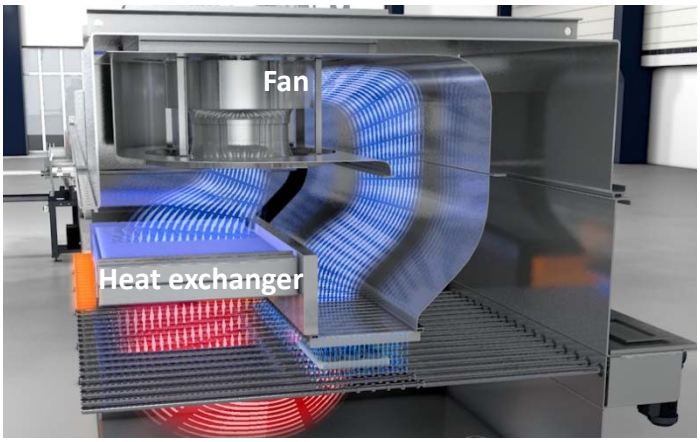

Fig. 3. Illustration of the cooling system.

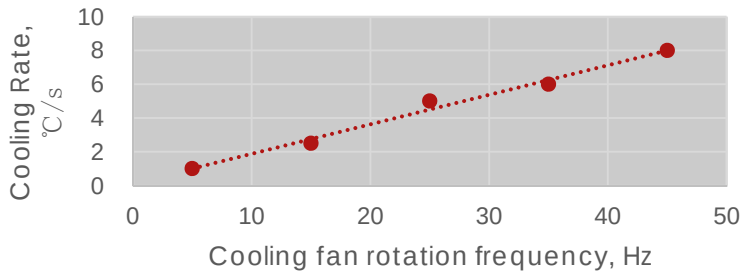

Fig. 4. The relationship between fan rotation speed and cooling rate.

After sintering, the gear specimens were tempered at a temperature of 200 ℃ for 1 hour in air to release the residual stress in a batch furnace.

The apparent hardness of the processed gear specimens was measured on the Rockwell B and C scale in the Zwick/Roell Zhu hardness tester. The apparent hardness was tested at the upper surface of the tooth shown in Figure 2. The distribution of the hardness from the tooth surface to the centre in the cross section was detected by the Zwick/Roell Zhu hardness tester.

The samples were cut from the processed gears and then polished and etched with Picral 4% and Nital 1% alcohol solutions for microstructure observation. The optical metallography was observed using a Leica DM4000M.

Results and discussion

The apparent hardness of the processed gears in different materials is shown in Figure 5. In general, the apparent hardness increased when using an increased cooling rate because of a higher martensite [10] content. In Figure 5 it can also be seen that the hardness in Gear A is higher than in Gear B and Gear C for the same material, and at the same cooling rate.

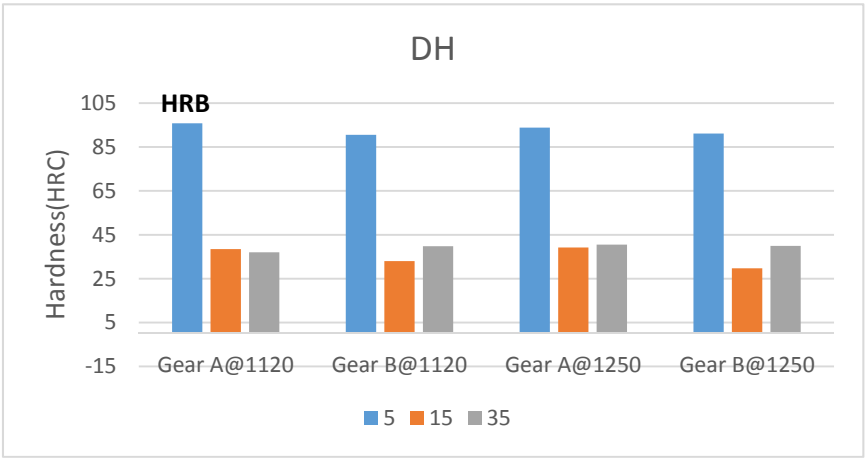

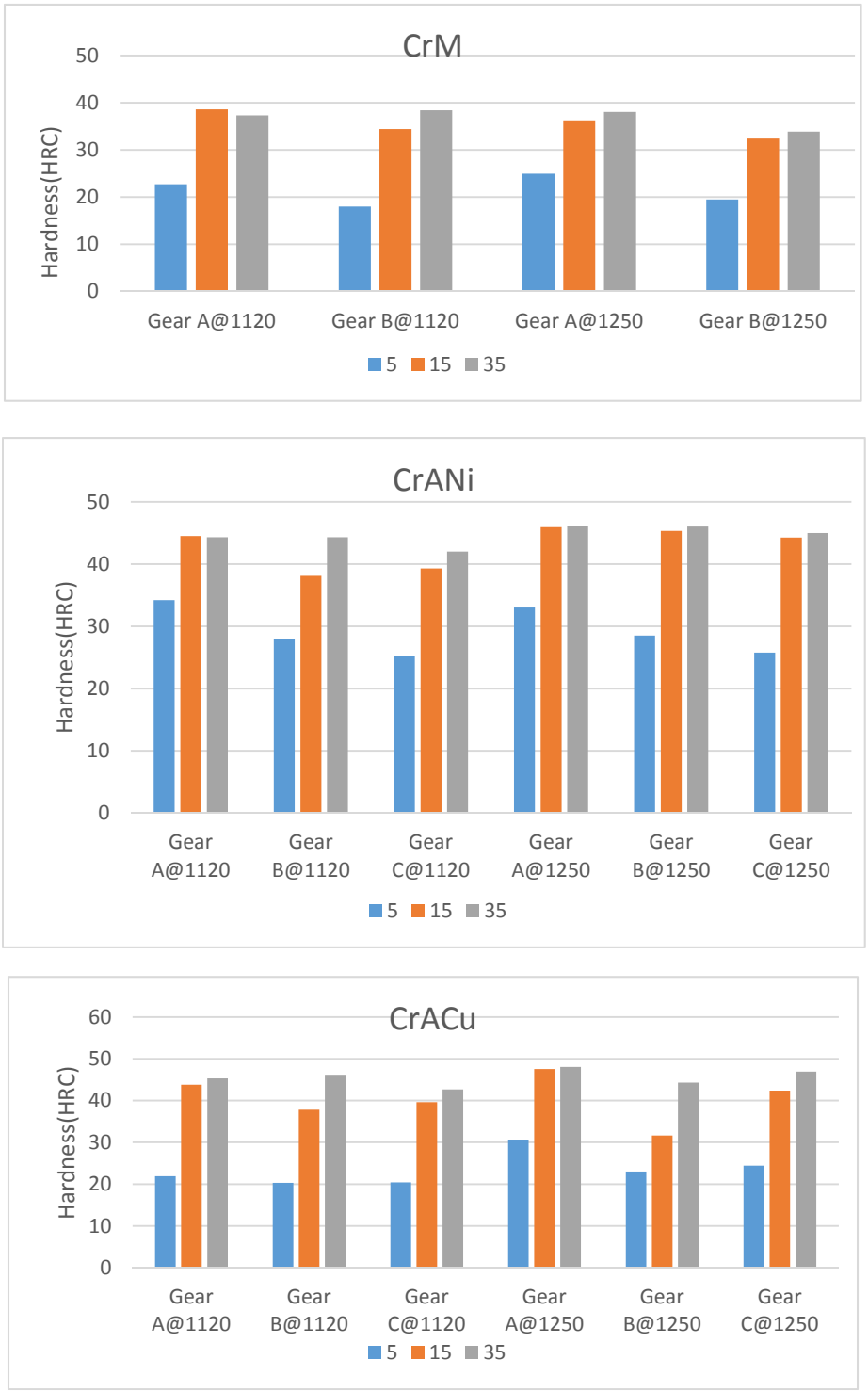

Fig. 5. Apparent hardness of processed gear specimens in different materials.

The surface area and mass of different gears was measured to investigate the effect of the mass and geometry upon performance,. The results are shown in Table 3. It is well known that more surface area and less mass will contribute to a faster cooling rate and an increase in martensite. To determine the effect of the mass and geometry upon the gear's performance after sinter-hardening the factor S/M, representing the surface area divided by mass is used.

Table 3. Mass, surface area and S/M of the gear specimens.

	Mass(g)	S(mm^2)	S/M(mm^2/g)
Gear A	500	17948	36
Gear B	800	16454	20
Gear C	1000	18965	19

The relationship between S/M and hardness with different cooling rates in different materials is shown in Figure 6. The surface area and unit weight is represented by S/M in physics. Increasing the S/M value results in higher thermal exchange properties which is good for the real cooling rate of the components. In Gear A, a higher S/M value created more thermal exchange and a higher martensite content. This also resulted in higher hardness and an S/M value of 36. Gear B and Gear C have the almost the same S/M value but Gear C has the bigger mass. High mass results in a high thermal capacity for the same materials at the same temperature when they cool down. Therefore, Gear C has a lower hardness when compared to Gear B.

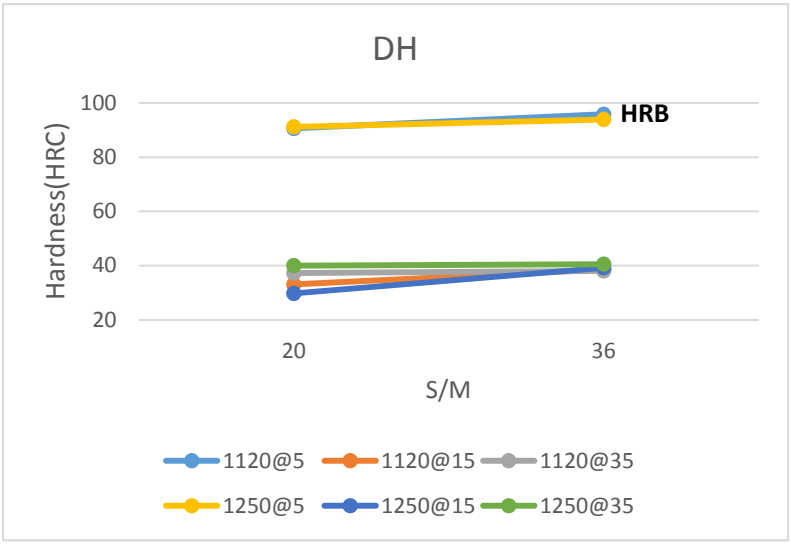

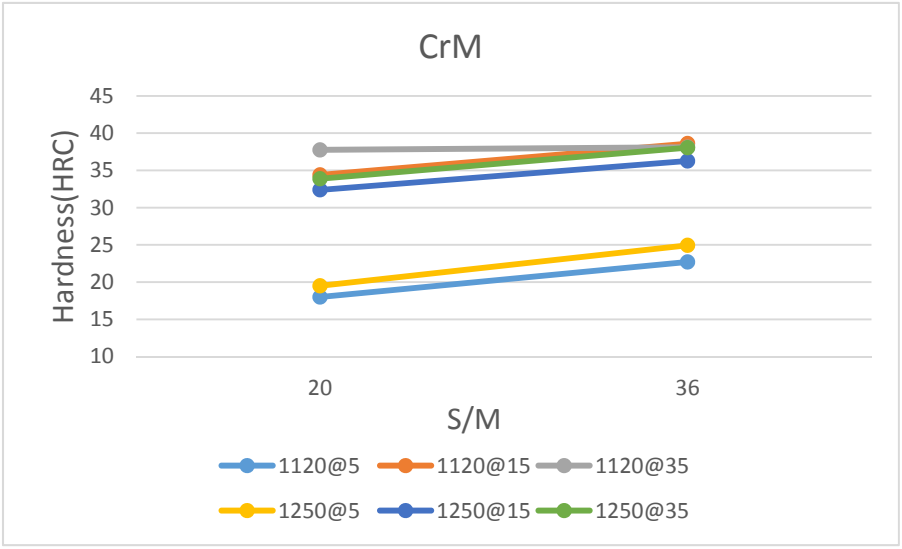

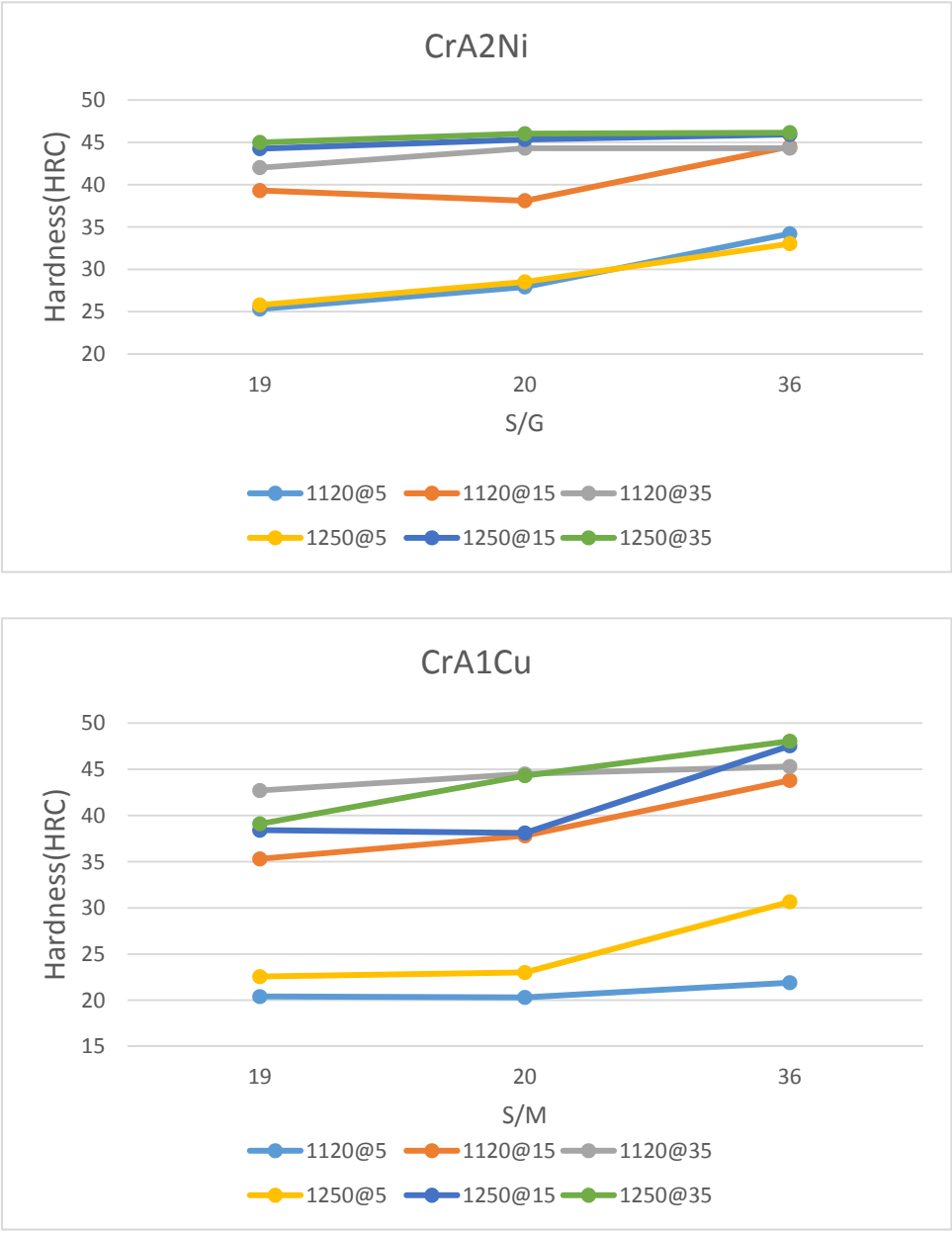

Fig. 6. Relationship between S/M and hardness in different materials.

In Figure 7 the distribution of apparent hardness for DH along the surface at different cooling rates is shown. In general, the hardness in Gear A is higher than Gear B. The hardness gap in the centre is smaller than near the surface because the cooling rate near the surface largely depends on the thermal exchange between the PM steel and the cooling atmosphere. It can also be seen that the hardness gap at the cooling rate of 6 ℃/s is smaller than others as they are almost both martensitic after this high cooling rate.

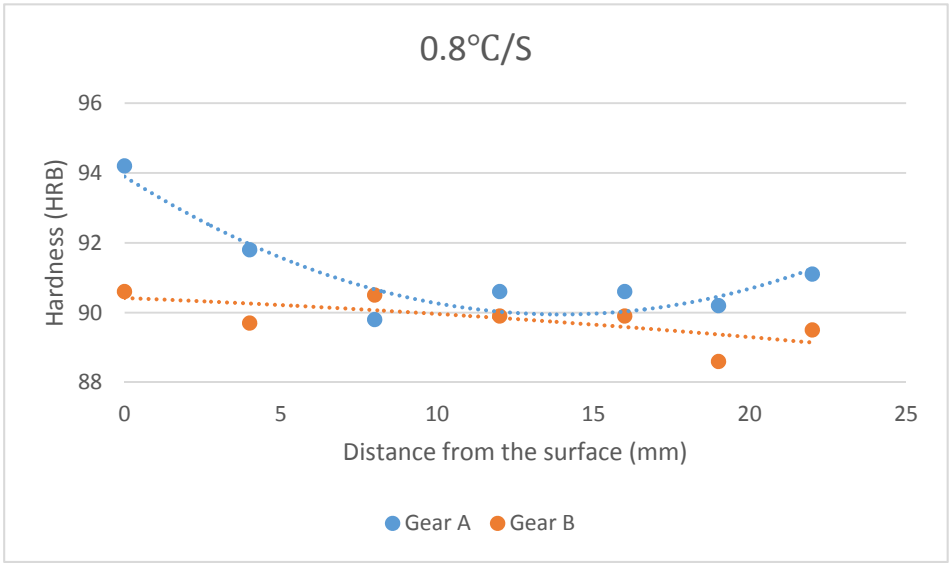

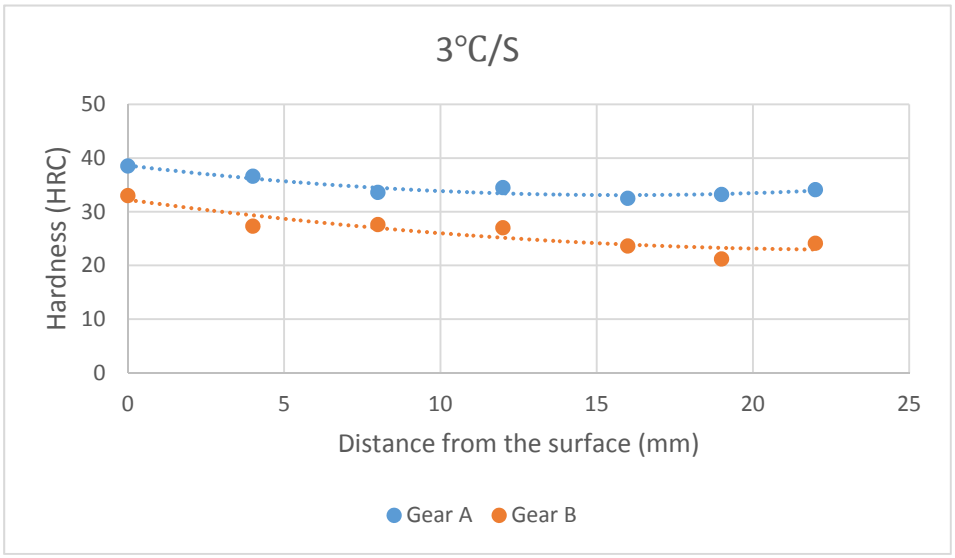

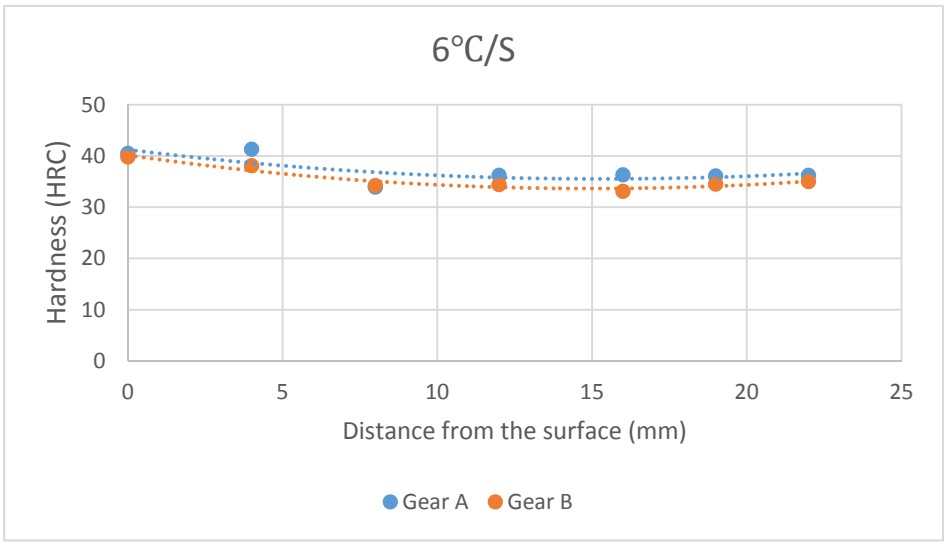

Fig. 7 Distribution of hardness along the surface of DH.

In Figure 8 you can see the microstructures of Gear A and Gear B in DH after different cooling rates. The different phase contents for both gears in DH are presented in Table 3. As expected, an increase in cooling rate created a higher martensite content. It can also be seen that the amount of martensite in Gear A is higher than that in Gear B when both are cooled at the same rate. This is due to a higher S/M value in Gear A than in Gear B. This also contributes to the different distribution of hardness between gear A and Gear B.

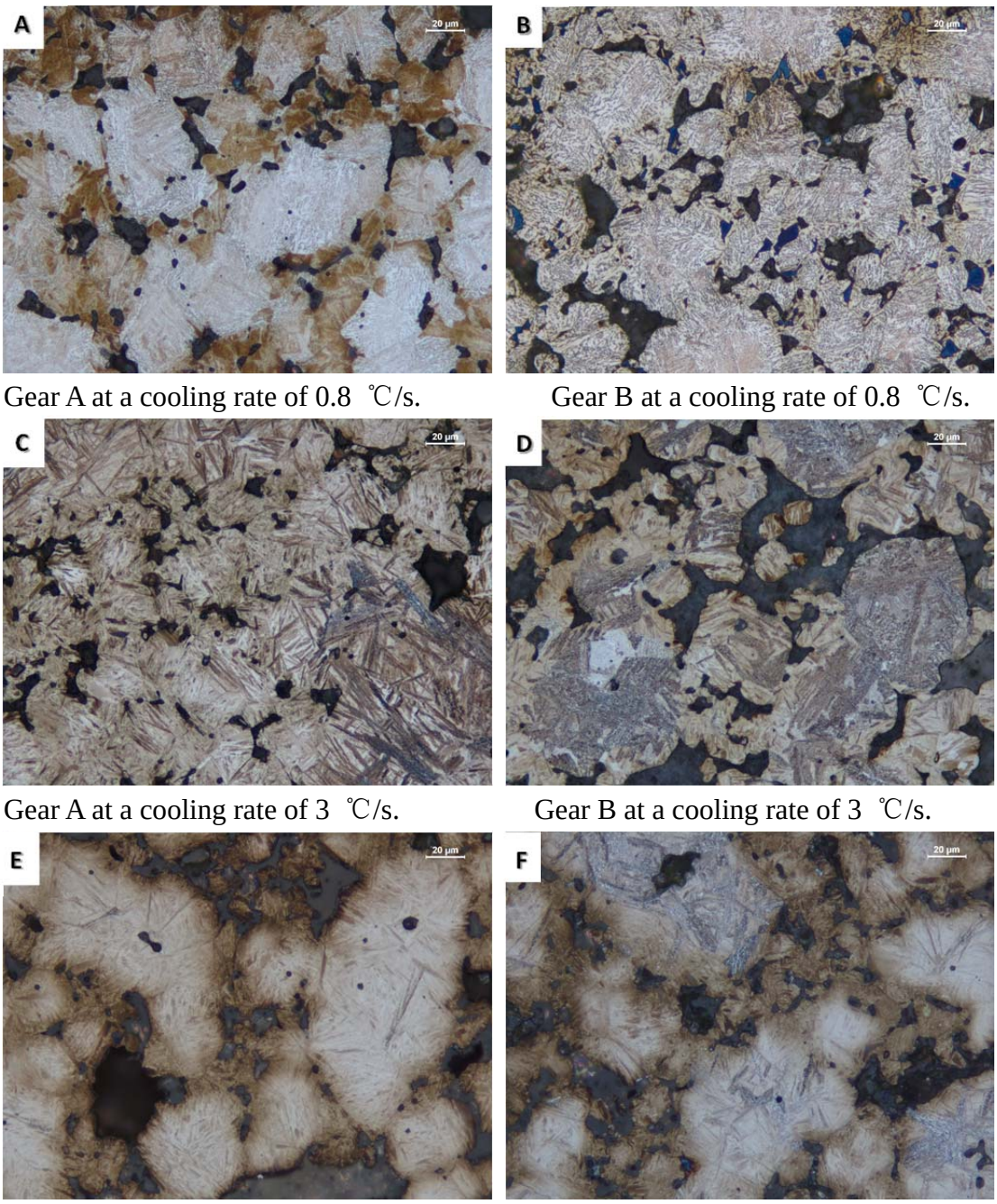

Gear A at a cooling rate of 0.8 ℃/s. Gear B at a cooling rate of 0.8 ℃/s.

Gear A at a cooling rate of 3 ℃/s. Gear B at a cooling rate of 3 ℃/s.

Gear A at a cooling rate of 6 ℃/s. Gear B at a cooling rate of 6 ℃/s.

Fig. 8. Microstructures of DH at different cooling rates.

Table 3. Phase contents from Figure 8.

		Martensite%	Bainite%
Gear A	0.8℃/s	10	90
	3℃/s	85	15
	6℃/s	98	2
Gear B	0.8℃/s	2	98
	3℃/s	40	60
	6℃/s	75	25

Conclusion

Gears made with DH, CrM, CrANi and sintered at different cooling rates by the new sinter-hardening furnace, showed that mass and geometry have an affect upon performance.

The apparent hardness increased when the cooling rate was increased due to a higher content of martensite.

The factor S/M, representing the surface area divided by mass, was used to detect the effect of mass and geometry upon performance after sinter hardening. Hardness in Gear A was higher than Gear B and Gear C, when using the same processing conditions because a higher S/M value created a better thermal exchange and resulted in more martensite content.

Hardness in Gear B was higher than Gear C despite the similar S/M value, because Gear C has a higher weight.

References

[1] J. Yang, J. Wang, Y. Han, S. Niu, O. Litstrom and L. Chen, Sinter-hardening PM Steels with Improved Dimensional Consistency for High Performance Components, Presented at PM2014 World Congress, Orlando, America
[2] M. L. Marucci, G. Fillari, P. King and K. S. Narasimhan, A review of current sinter-hardening technology, Presented at PM2004 World Congress, Vienna, Austria.
[3] U. Engstrom, R. Frykholm, D. Milligan and R. Warzel, Cost effective materials for sinter hardening applications, Presented at PM2008 World Congress, Washington, America.
[4] C. Larsson, U. Engstrom and S. Berg, Means to Lift Mechanical Properties to the Next Level, Enabling New Challenging, Presented at EURO PM2012, Basel, Switzerland
[5] S. Hatami, A. Malakizadi, L. Nyborg and D. Wallin, Critical aspects of sinter-hardening of prealloyed Cr–Mo steel, J. of Mater. Processing Tech., 210(2010)1180-1189.
[6] Y. Yu, Sinter hardening - a big Market and Technology Potential in China,

Presented at PMAsia2007, Shanghai, China
[7] M. Gagne, Y. Trudel, Effects of Post-sintering Cooling on the Properties of Low Alloy Sintered Materials, Advances in powder Metallurgy and Particulature Materials-1991, MPIF, Princeton, America.
[8] U. Engstrom, Evaluation of Sinter Hardening of different PM materials, Not published.
[9] K. S. Moghaddam, M Ghambari, H. Farhangi and N. Solimanjad, Effect of Sinter Hardening on Microstructure and Mechanical Properties of Astaloy 85Mo, J. of Iron and Steel Research, International, 19(2012)43-46.
[10] F. J. Semel, Cooling Rate Effects on the Metallurgical Response of a Recently Developed Sintering Hardening Grade, Presented at PM^{2}TEC 2002, Orlando, America.